IEEE Access
Multidisciplinary | Rapid Review | Open Access Journal

Received February 18, 2021, accepted March 9, 2021, date of publication March 10, 2021, date of current version March 22, 2021.

Digital Object Identifier 10.1109/ACCESS.2021.3065577

Chance-Constrained Optimal Distribution Network Partitioning to Enhance Power Grid Resilience

SHUCHISMITA BISWAS, (Graduate Student Member, IEEE), MANISH K. SINGH, (Graduate Student Member, IEEE), AND VIRGILIO A. CENTENO, (Senior Member, IEEE)

Department of Electrical and Computer Engineering, Virginia Tech, Blacksburg, VA 24060, USA

Corresponding author: Shuchismita Biswas (suchi@vt.edu)

This work was supported in part by the Virginia Tech Open Access Subvention Fund.

ABSTRACT This article proposes a method for identifying potential self-adequate sub-networks in the existing power distribution grid. These sub-networks can be equipped with control and protection schemes to form microgrids capable of sustaining local loads during power systems contingencies, thereby mitigating disasters. Towards identifying the best microgrid candidates, this work formulates a chance-constrained optimal distribution network partitioning (ODNP) problem addressing uncertainties in load and distributed energy resources; and presents a solution methodology using the sample average approximation (SAA) technique. Practical constraints like ensuring network radiality and availability of grid-forming generators are considered. Quality of the obtained solution is evaluated by comparison with- a) an upper bound on the probability that the identified microgrids are supply-deficient, and b) a lower bound on the objective value for the true optimization problem. Performance of the ODNP formulation is illustrated through case-studies on a modified IEEE 37-bus feeder. It is shown that the network flexibility is well utilized; the partitioning changes with risk budget; and that the SAA method is able to yield good quality solutions with modest computation cost.

INDEX TERMS Chance-constrained optimization, microgrid, grid-forming generators, radiality, resilience.

NOMENCLATURE

Unless specified otherwise, boldface symbols represent vectors and matrices, while calligraphic symbols denote sets. A non-exhaustive list of main symbols follows.

$(\boldsymbol{x}, \boldsymbol{\xi})$	Decision variables and uncertain parameters
ε	Tunable risk parameter
$\mathcal{G}_N$	Power distribution network graph
$(\mathcal{V}_N, \mathcal{E}_N)$	Vertex and edge set for $\mathcal{G}_N$
$\mathcal{G}$	Subgraph of $\mathcal{G}_N$ that omits substation vertex
$(\mathcal{V}, \mathcal{E})$	Vertex and edge set for $\mathcal{G}$
$e_{i,j}$	Edge connecting vertices i and j
$(\xi_i^{d_p}, \xi_i^{d_q})$	Active/reactive power demand at bus i
$(\xi_i^{g_p}, \xi_i^{g_q})$	Active/reactive generation capacity at bus i
v_i	Voltage magnitude at bus i
(p_i, q_i)	Active/reactive power injection at bus i
b_i^n	Binary on/off status of bus i
b_{ij}^e	Binary on/off status of line e_{ij}
(P_{ij}, Q_{ij})	Active/reactive power flow on line e_{ij}
P_{ij}^{max}	Active power flow limit on line e_{ij}
Q_{ij}^{max}	Reactive power flow limit on line e_{ij}
(p_i^g, q_i^g)	Active/reactive generation at bus i
(p_i^d, q_i^d)	Active/reactive demand at bus i
(r_{ij}, x_{ij})	Resistance/reactance of line e_{ij}
$(\tilde{\mathbf{A}}, \mathbf{A})$	Full/reduced branch-bus incidence matrix
$(\mathbf{f}, \mathbf{f}')$	Virtual line flows
$\boldsymbol{\theta}$	Binary indicator on edge set
$\mathcal{V}_s$	Set of buses with grid-forming capabilities
$\boldsymbol{\psi}_1$	Set of variables that are fixed across scenarios
$\boldsymbol{\psi}_2$	Set of scenario-dependent variables
γ	Risk level for the SAA problem
$q(\boldsymbol{x})$	Probability of chance constraint violation

The associate editor coordinating the review of this manuscript and approving it for publication was Giambattista Gruosso.

I. INTRODUCTION

In recent years, the adoption of renewable energy based distributed energy resources (DERs) has increased due to the recognition of their economic and environmental benefits.

A primary advantage of DERs is their ability to sustain local loads if the main grid is lost, possibly due to natural disasters. DERs and loads may be clustered together to form *microgrids* which supply essential loads and aid service restoration during and after outages, thereby boosting grid resilience [1]. According to the IEEE 1547.4-2011 standard, microgrids: *1)* have DERs and load; *2)* can operate in both grid-connected and islanded modes; and *3)* are intentionally planned [2].

Historically, industrial customers have used diesel generators (DGs) to ensure emergency power supply. However, other DER options such as solar generators can also provide efficient, onsite energy [3]. Similarly, combined heat and power plants (CHP) can alleviate grid stress and reduce the energy cost at industrial sites [4]. As CHPs are 'always-on' units primarily run to serve industrial needs, they can be quickly deployed to provide grid-support during stressed conditions. The energy storage capacity of modern electric vehicles (EVs) may also be exploited to enhance grid resilience [5]. Reference [6] suggests that EVs can be encouraged to interact with the grid through incentivized charging schemes offered by public parking lots. Such parking lots often have a large number of EVs parked at a time. Thus, under a suitable policy framework, utilities may tap into their stored energy during emergencies. A promising direction for using electric buses as mobile energy storage units is explored in [7]. As larger EVs like buses and trucks have very high storage capacity, they can be proactively dispatched as back-up generators to aid areas facing natural disasters. Hence, fixed and mobile DERs provide multiple avenues to boost grid resilience, and effective strategies should be designed to utilize them.

Note that isolated DERs cannot supply local loads if they lack adequate protection and control capabilities. When DERs are inadvertently separated from the grid (a condition called *unintentional islanding*), electric utilities cannot regulate the voltage and frequency in the unplanned islands. Voltage and/or frequency excursions outside prescribed limits may severely damage system loads and also pose safety concerns. Hence, several measures to detect and avoid unintentional islanding have been developed [8]. On the other hand, the generation capacity of DERs may be exploited to mitigate outages if they can be designed to operate safely in islanded conditions. Therefore, utilities are interested in identifying potential candidates within existing active distribution networks that can be converted to microgrids via economically viable retrofitting. Microgrids need to be equipped with adequate switching, protection and control mechanisms prior to any expected outage. Thus, optimally splitting a network into microgrids constitutes a pertinent planning problem [9]–[15].

This optimal distribution network partitioning (ODNP) task seeks to identify potential *self-adequate* sub-networks that can survive the loss of the main grid as islands. Both exact [9]–[11] and heuristic [12]–[15] methods have been proposed in literature to address the ODNP problem. Self-adequacy in the objective function has been surrogated by either expected load-generation imbalance within microgrids [13]–[15], or expected power flow on boundary lines [9]–[12]. Some works additionally suggest dynamic identification of boundary lines in response to faults [16], [17]. However, since distribution networks are only served by a limited number of switching devices at present, implementing these suggestions may be difficult in practice. A method for determining self-sufficient islands in transmission networks is described in [18], but cannot be directly extended to ODNP without including distribution system specific constraints.

Distribution networks are usually operated in a radial fashion for protection coordination, and this radiality needs to be maintained in microgrids as well. In [11], [13]–[15], ODNP is demonstrated on an already radial feeder and radiality conditions are not explicitly enforced. This approach ignores the presence of normally open switches that allow network reconfiguration, thereby under-utilizing grid flexibility. Radiality is considered in [10], but another restrictive condition is imposed- eacha microgrid is assigned exactly one DER. This single DER constraint is also present in [16]. In this approach, the number of partitions are predetermined, leading to sub-optimal solutions. A radiality constraint without specifying the number of microgrids was recently presented in [9], and the formulation in the current work builds upon this approach.

A critical aspect that has been overlooked in the existing microgrid planning literature is the requirement of grid-forming generators in viable islands. The IEEE 1547.4-2011 standard mandates that an island should have at least one generator that provides voltage and frequency support during a system disturbance, or has black-start capabilities [2]. An exhaustive path search based method for checking connectivity to black-start generators has been proposed in [19]. Another multiple commodity flow based approach outlined in [20] separately checks nodes for their connectivity to black-start nodes. Both these approaches become computationally prohibitive for large meshed networks. The ODNP formulation put forth in the present work guarantees that all nodes in each microgrid will be connected to at least one grid-forming generator. The formulation is somewhat similar to the single commodity flow model of [20] but uses fewer constraints and shows faster performance (empirically observed to be 10 to 20% faster).

ODNP is further complicated by the fact that power demands and renewable energy generation are stochastic in nature. In [11], [13]–[15], [17], the uncertainty in load and generation is addressed by constructing typical daily profiles, over which optimization is performed. However, the quality of solution obtained is not evaluated. The present work formulates a chance-constrained ODNP (cc-ODNP) to identify optimal microgrids in the planning stage. This is computationally challenging as the underlying deterministic optimization problem is combinatorial, and is formulated as a non-convex mixed integer linear program (MILP). To ensure computational tractability, a sampling and integer programming based strategy has been used to solve an approximation

of the cc-ODNP, and the quality of the solution obtained is rigorously evaluated using statistical tools [21].

The main contributions of this work are stated next.

- First, a deterministic ODNP problem for identifying optimal microgrids given real-time load-generation values is formulated. This formulation comprehensively addresses operational constraints, including: *a)* maintaining network radiality, and *b)* ensuring every microgrid includes a grid-forming generator, without any pre-assignment. The requirement of grid-forming generators has not been addressed in the existing work on microgrid planning.
- Second, the ODNP formulation is extended to a probabilistic setup, and solved using a computationally tractable sample average approximation (SAA) method. Quality of an obtained solution is evaluated considering: a) an upper bound on the probability that the candidate microgrids are supply-deficient, and b) a lower bound on the objective value for the probabilistic optimization problem.
- Third, the ODNP formulation is evaluated through extensive numerical tests on a modified IEEE 37-bus feeder. It is shown that the SAA approach is able to efficiently utilize network flexibility, and outperforms a robust clustering based method in terms of objective cost.

The remainder of the article is organized as follows. Section II briefly examines how the present work quantitatively enhances power systems resilience. Section III introduces some mathematical preliminaries. Section IV describes the ODNP formulation. The underlying deterministic problem is established first, and then probabilistic constraints arising from the uncertainty in load an generation are added. Section V discusses the mathematical tools used to assess the quality of the obtained ODNP solution. Section VI details the numerical experiments conducted to validate the performance of the ODNP formulation. Section VII concludes the article and outlines future research directions.

II. POWER SYSTEMS RESILIENCE

Resilience may be defined as the ability of a system to prepare for, respond to and recover from natural and man-made disasters. Recent natural disasters have exposed vulnerabilities in the power systems infrastructure, necessitating strategies to enhance its resilience. However, to evaluate the effectiveness of competing strategies, some quantitative measure for capturing the rather conceptual idea of resilience is required. Several recent research efforts have sought to describe resilience in quantitative terms and model the inter-dependencies between power systems and other critical infrastructure sectors [22]–[24].

A popular approach to quantify resilience builds around the multi-phase resilience trapezoid that depicts system behavior during a disaster; see fig. 1. Consider a disruptive event that starts at time t_e. This *first phase* ($t \in [t_e, t_d]$) of event progress is characterized by an ongoing deterioration in system performance from its pre-disturbance levels. In the *second phase* ($t \in [t_d, t_r]$), the system operates in a diminished capacity for some time before restoration steps can be initiated.

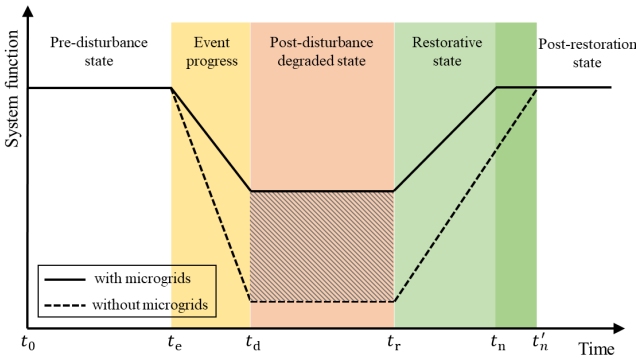

FIGURE 1. Multi-phase resilience trapezoid, adapted from [22].

During the *third phase* ($t \in [t_r, t_n]$), actions are taken to restore the system to its pre-event performance levels. The transitions between system states in fig. 1 are linear only for expository convenience. In practice, these may be non-linear, depending on system characteristics, prevalent conditions and the nature of the disaster.

Note that in fig. 1, the y-axis represents a generic system function as its performance measure. Different quantities have been used to convey system performance, for example, reference [23] considers the power supplied to critical loads weighted by their criticality. The formulation presented in this article considers the total load served by microgrids once the main grid is lost. Maximizing microgrid service will in turn reduce load interruptions and boost traditional grid reliability measures such as SAIDI (System Average Interruption Duration Index), SAIFI (System Average Interruption Frequency Index) and MAIFI (Momentary Average Interruption Frequency Index) [25].

The resilience trapezoid describes - a) the rate and extent of performance drop when a disruptive event strikes, b) how long the system resides in a degraded state, and c) how fast it recovers to the pre-disturbance state. A metric that combines these measures and quantifies the resilience of a system is the *area under the curve (AUC)* of the trapezoid. Any resilience enhancement strategy attempts to maximize this AUC. Figure 1 shows how ODNP proposes to increase the AUC of the resilience trapezoid. As shown by the dotted line, if a distribution network is not equipped with microgrids, a loss of the grid may result in a drastic decrease in load served despite installed DER capacity. By optimally planning microgrids with existing DERs, the system behavior can be changed to the solid line shown in fig. 1. The proposed ODNP formulation maximizes the load served during the degraded state of second phase. Thus, the shaded portion shown in the second phase of the resilience trapezoid is evidently maximized, thereby increasing the AUC. Further, by improving system performance in the degraded state, one can anticipate a faster recovery (from t'_n to t_n in fig. 1), further increasing the AUC. Of course, the recovery time will depend on multiple factors such as time and nature of disturbance, pre-event system operating state etc. Nevertheless, the ODNP formulation provides a general methodology for enhancing

distribution network resilience, that can be adapted to incorporate different DER technologies.

III. PRELIMINARIES

In this section, some mathematical preliminaries are revisited before expounding on the problem formulation. Standard mathematical notations are used, calligraphic symbols represent sets, lower (upper) case bold letters represent column vectors (matrices). All zero and all one vectors and matrices of appropriate size are denoted by $\mathbf{0}$ and $\mathbf{1}$ respectively.

A. GRAPH THEORY

A graph $\mathcal{G} := (\mathcal{V}, \mathcal{E})$ consists of a *vertex set* $\mathcal{V}$ and an *edge set* $\mathcal{E}$, where an edge is an unordered pair of distinct vertices of $\mathcal{G}$. Edge $e_{ij} \in \mathcal{E}$ is denoted by its incident vertices (i, j), such that $i, j \in \mathcal{V}$. If $e_{ij} \in \mathcal{E}$, then vertices i and j are *adjacent*. Two edges are adjacent if they have a common vertex. A *subgraph* of $\mathcal{G}$ is a graph $\mathcal{H} := (\mathcal{X}, \mathcal{Y})$ such that $\mathcal{X} \subseteq \mathcal{V}$ and $\mathcal{Y} \subseteq \mathcal{E}$. If $\mathcal{X} = \mathcal{V}$, then $\mathcal{H}$ is a *spanning subgraph* of $\mathcal{G}$. $\mathcal{H}$ is an *induced subgraph* of $\mathcal{G}$ if vertices in $\mathcal{X}$ are adjacent in $\mathcal{H}$ if and only if they are adjacent in $\mathcal{G}$.

A *path* from i to j is a sequence of distinct vertices starting at i and ending at j such that consecutive vertices are adjacent. If there is a path between all pairs of vertices of a graph $\mathcal{G}$, then $\mathcal{G}$ is *connected*; else $\mathcal{G}$ is *disconnected*. An induced subgraph of $\mathcal{G}$ that is maximal, subject to being connected, is called a *connected component* of $\mathcal{G}$. A *cycle* is a sequence of adjacent edges without repetition that starts and ends at the same node. A graph with no cycles is called *acyclic*. A connected and acyclic graph is a *tree*. A *spanning tree* subgraph of $\mathcal{G}$ is a tree that covers all vertices in $\mathcal{G}$. An acyclic graph with multiple connected components is a *forest*. A *spanning forest* subgraph of $\mathcal{G}$ is a forest that covers all vertices in $\mathcal{G}$. Spanning forests may include connected components with a single node. For further reference, a review of graph theory fundamentals is available in [26].

B. CHANCE-CONSTRAINED OPTIMIZATION

Stochastic optimization refers to a collection of methods for solving an optimization problem with uncertain parameters. For many real-world applications operating in uncertain environments, ensuring 100% reliability is physically and economically impractical. This difficulty is often dealt with by designing systems that assure a minimum reliability level with high probability. Mathematical models of such reliability-constrained systems involve the use of probabilistic or *chance constraints* [21]. A generic chance-constrained optimization (CCO) problem is of the form:

$$\min_{\boldsymbol{x} \in \mathcal{X}} f(\boldsymbol{x}) \tag{P_1}$$

$$\text{s. to } \boldsymbol{h}(\boldsymbol{x}) \leq \mathbf{0} \tag{C_1}$$

$$Pr\{\boldsymbol{g}(\boldsymbol{x}, \boldsymbol{\xi}) \leq \mathbf{0}\} \geq 1 - \varepsilon \tag{C_2}$$

Here, $\boldsymbol{x}$ is the vector of decision variables, whose feasible region is given by $\mathcal{X} \subset \mathbb{R}^n$. The objective function to be minimized is $f : \mathbb{R}^n \to \mathbb{R}$. Vector $\boldsymbol{\xi}$ stacks the uncertain parameters with known probability distribution, and $\varepsilon \in (0, 1)$ is a tunable risk parameter. Problem P_1 seeks to find an optimal decision vector $\boldsymbol{x}^*$ that minimizes $f(\boldsymbol{x})$, such that the *hard constraints* C_1 are always satisfied, while the *chance constraint* C_2 is satisfied with probability at least $1 - \varepsilon$.

In power systems literature, CCO has been previously used to address security constrained economic dispatch and unit commitment problems [27]. This class of problems is difficult to solve, due to two main reasons:

- Given a candidate solution $\bar{\boldsymbol{x}} \in \mathcal{X}$, accurately computing $Pr\{\boldsymbol{g}(\bar{\boldsymbol{x}}, \boldsymbol{\xi}) \leq \mathbf{0}\}$ can be very difficult, making it hard to check if constraint C_2 is satisfied.
- The feasibility region defined by a chance constraint is usually not convex [21]. This makes finding an optimal solution difficult even when the feasibility of $\bar{\boldsymbol{x}}$ can be checked.

These difficulties may be overcome by considering a *sample average approximation* (SAA) of the original problem where the true distribution of $\boldsymbol{\xi}$ is replaced by an empirical distribution with discrete support. The SAA is still a chance-constrained stochastic problem, but with a different distribution for $\boldsymbol{\xi}$, and may be solved via integer programming [21]. This method has been shown to yield good candidate solutions if the sampling is ample and rich. In this work, the SAA approach will be incorporated to solve a probabilistic ODNP and the solution obtained will be further analyzed to verify how well it solves the original optimization problem.

IV. PROBLEM FORMULATION

Given a distribution network with DERs, planners would like to optimally construct microgrids, such that the DERs are able to sustain internal loads if supply from the main grid is lost. Load served is to be maximized. Both load and generation vary with the weather and assuring self-adequacy for the worst case may lead to very conservative solutions. Hence, a solution that works well for *most* operating conditions might be preferable. Thus microgrids may be designed to be self-adequate with probability at least $(1 - \varepsilon)$ across all possible operating scenarios, where ε is a tunable risk parameter. The value of ε may be chosen based on several factors such as available storage resources. Once optimal microgrids are identified, they need to be equipped with control capabilities and boundary line switches. It must be noted that depending on the generation capacity of installed DERs, all load in a network may not be served by microgrids.

Our mathematical formulation is put forth in three steps. First, a deterministic version of the problem, d-ODNP is presented where the load served is maximized for a given scenario of demands and generation. Next, the chance constraints arising from the randomness in generation and demands are added. Finally, a SAA based algorithm is proposed that can tractably solve the probabilistic ODNP.

A. DISTRIBUTION NETWORK MODEL

A single-phase distribution network may be represented by a connected directed graph $\mathcal{G}_N := (\mathcal{V}_N, \mathcal{E}_N)$, where vertices denote buses and edges denote lines. The substation node is

indexed by 0; and the set of all other nodes is denoted by $\mathcal{V} := \mathcal{V}_N \setminus \{0\}$. Each edge $e_{i,j} \in \mathcal{E}_N$ is assigned an arbitrary direction from node i to j. If $e_{i,j} \in \mathcal{E}_N$, then $e_{j,i} \notin \mathcal{E}_N$. The task at hand considers that the main grid is unavailable, hence partitioning needs to be carried out on $\mathcal{G} := (\mathcal{V}, \mathcal{E})$, the induced subgraph of $\mathcal{G}_N$ on vertex set $\mathcal{V}$. In the present setup all lines are considered switchable. Any non-switchable edge coinciding with a microgrid boundary would need to be retrofitted with a switch. Moreover, graph edges include lines with existing normally open and normally closed switches, and hence $\mathcal{G}$ is not necessarily radial.

Each node has an associated demand $(\xi_i^{d_p} + j\xi_i^{d_q})$ and generation capacity $(\xi_i^{g_p} + j\xi_i^{g_q})$. The demand and generation capacities are not precisely known at the planning stage and only a probability distribution, possibly empirical, may be available. Let v_i be the voltage magnitude at bus i and $(p_i + jq_i)$ be the complex power injection. Bus voltages, demand, generation capacity, and complex power injections are respectively stacked into vectors $\mathbf{v}$, $\boldsymbol{\xi}^{\boldsymbol{d_p}} + j\boldsymbol{\xi}^{\boldsymbol{d_p}}$, $\boldsymbol{\xi}^{\boldsymbol{g_p}} + j\boldsymbol{\xi}^{\boldsymbol{g_q}}$, $\mathbf{p} + j\mathbf{q}$. All quantities are in per units.

Let us introduce binary variables b_i^n and b_{ij}^e that respectively dictate if vertex $i \in \mathcal{V}$ and edge $e_{ij} \in \mathcal{E}$ are energized. The end nodes i and j of an energized edge e_{ij} shall be energized, requiring

$$b_i^n + b_j^n \geq 2b_{ij}^e \quad \forall e_{ij} \in \mathcal{E}. \tag{1}$$

The ANSI standards mandate that voltages at energized buses should be within $\pm 5\%$ p.u. of the nominal value [28]. Thus,

$$0.95\, \mathbf{b^n} \leq \mathbf{v} \leq 1.05\, \mathbf{b^n}. \tag{2}$$

Let the power flow on line $e_{ij} \in \mathcal{E}$ be $P_{ij} + jQ_{ij}$. The line capacity constraints may be formulated as follows.

$$-b_{ij}^e P_{ij}^{max} \leq P_{ij} \leq b_{ij}^e P_{ij}^{max} \quad \forall e_{ij} \in \mathcal{E} \tag{3a}$$
$$-b_{ij}^e Q_{ij}^{max} \leq Q_{ij} \leq b_{ij}^e Q_{ij}^{max} \quad \forall e_{ij} \in \mathcal{E} \tag{3b}$$

Flow constraints of the form $P_{ij}^2 + Q_{ij}^2 \leq S_{ij}^2$ (where S denotes apparent power) are not used here to avoid quadratic constraints. A polytopic approximation of this constraint proposed in [29] could also be used.

B. POWER FLOW MODEL

DER units plausible in a low/medium voltage distribution network setup include photo-voltaic (PV) generators, diesel generators (DGs) and combined heat and power plants (CHPs). The active power generation capacity of these units maybe stochastic; for instance PV generation is dictated by solar irradiance levels, and CHP generation is affected by local heating demands. Non-utility scale PV generators are usually not dispatchable, while some DER units like CHPs may be dispatchable limited by their stochastic generation capacity. DG units are usually dispatchable and their maximum generation capacity may be fixed based on the machine rating. Loads are assumed to be inelastic.

The power generations by dispatchable units are governed by the following equations:

$$0 \leq p_i^g \leq b_i^n \xi_i^{g_p} \quad \forall i \in \mathcal{V}_D \tag{4a}$$
$$-b_i^n \xi_i^{g_q} \leq q_i^g \leq b_i^n \xi_i^{g_q} \quad \forall i \in \mathcal{V}_D. \tag{4b}$$

Here, constraints (4a)-(4b) bound the generator outputs p_i^g, q_i^g at bus i. Set $\mathcal{V}_D$ comprises of all nodes with a dispatchable generator. Given the limit on active power, a corresponding limit on reactive power generation can be obtained based on the generator apparent power ratings. Non-dispatchable generators are incorporated into the formulation as shown below.

$$p_i^g = b_i^n \xi_i^{g_p} \quad \forall i \in \mathcal{V} \setminus \mathcal{V}_D \tag{5a}$$
$$q_i^g = b_i^n \xi_i^{g_q} \quad \forall i \in \mathcal{V} \setminus \mathcal{V}_D \tag{5b}$$

Constraints (5a)-(5b) state that the power output by an energized non-dispatchable DER is equal to its stochastic generation capacity. For inelastic loads, the constraints for power consumption become:

$$p_i^d = b_i^n \xi_i^{d_p} \quad \forall i \in \mathcal{V} \tag{6a}$$
$$q_i^d = b_i^n \xi_i^{d_q} \quad \forall i \in \mathcal{V} \tag{6b}$$

Constraints (6a)-(6b) state that consumption at bus i is equal to its demand; if energized. Thus the net power injections are:

$$p_i = p_i^g - p_i^d \quad \forall i \in \mathcal{V} \tag{7a}$$
$$q_i = q_i^g - q_i^d \quad \forall i \in \mathcal{V} \tag{7b}$$

For power flow calculations, the linearized distribution flow (LDF) model proposed in [30] is followed. Despite being an approximation for the full AC power flow model, LDF has been used extensively and shown to perform well in literature [31]. Now, ignoring line losses, the power balance at each node entails:

$$\sum_{e_{ij} \in \mathcal{E}} P_{ij} - \sum_{e_{jk} \in \mathcal{E}} P_{jk} = p_j \quad \forall j \in \mathcal{V} \tag{8a}$$
$$\sum_{e_{ij} \in \mathcal{E}} Q_{ij} - \sum_{e_{jk} \in \mathcal{E}} Q_{jk} = q_j \quad \forall j \in \mathcal{V} \tag{8b}$$

Let $r_{ij} + jx_{ij}$ be the impedance of line $e_{ij} \in \mathcal{E}$. Then, the relationship between voltages and power injections may be linearized as: $v_i^2 - v_j^2 = 2(r_{ij}P_{ij} + x_{ij}Q_{ij})$. Assuming small voltage deviations, the squared terms may be approximated as $v_i^2 \simeq 2v_i - 1$. Using these results,

$$b_{ij}^e (v_i - v_j - r_{ij}P_{ij} - x_{ij}Q_{ij}) = 0, \quad \forall e_{ij} \in \mathcal{E} \tag{9}$$

Here, the indicator b_{ij}^e is multiplied to enforce the voltage drop relation only for energized lines. For computational ease, bilinear terms like $b_{ij}^e v_i$ in (9) can be handled by McCormick linearization, where the product terms are replaced by their linear convex envelopes to yield a relaxation of the original non-convex feasible set [32]. If at most one of the variables is continuous and the rest are binary, this relaxation is exact. For illustration, let us consider a term $z = xy$, where x is

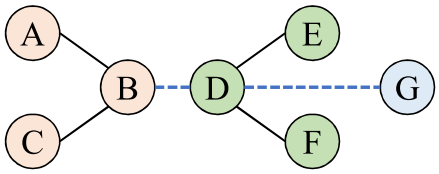

FIGURE 2. Components ($\{A, B, C\}$, $\{AB, BC\}$), ($\{D, E, F\}$, $\{DE, DF\}$) and ($\{G\}$, $\{\}$) form a spanning forest. Adding edges *BD* and *DG* creates a spanning tree.

binary and y is a continuous variable bounded in $y \in [\underline{y}, \bar{y}]$. Here, $z = xy$ may be equivalently expressed as four linear inequality constraints.

$$x\underline{y} \leq z \leq x\bar{y} \tag{10a}$$

$$y + (x-1)\bar{y} \leq z \leq y + (x-1)\underline{y} \tag{10b}$$

Note that putting $x = 0$ in equations (10a)-(10b) yields $z = 0$. Similarly, putting $x = 1$ yields $z = y$. All such bilinear terms appearing henceforth in this work will be treated similarly.

C. RADIALITY CONSTRAINTS

Network radiality is essential for distribution system operations. Some prior approaches proposed for enforcing radiality are cycle elimination [19] and virtual commodity flow [9], [33]. The ODNP task needs to identify $\mathcal{G}' = (\mathcal{V}, \mathcal{E}')$, a spanning subgraph of $\mathcal{G}$, such that every connected component, or simply component, of $\mathcal{G}'$ is a tree, i.e. $\mathcal{G}'$ is a *forest*. A spanning forest may include isolated nodes, i.e. it may have components with a single vertex and no edges.

As discussed in section I, the radiality formulation outlined in this article has the following advantages: a) the optimal number of microgrids and their topologies are determined in a single-shot, and b) DERs need not be pre-assigned to microgrids like in [10], [16]. The radiality constraints will be formulated using the following proposition.

Proposition 1 [9]: Given a spanning forest subgraph $\mathcal{F} := (\mathcal{V}, \mathcal{E}_F)$ of a connected graph $\mathcal{G} := (\mathcal{V}, \mathcal{E})$, there exists at least one spanning tree subgraph of $\mathcal{G}$, expressed as $\mathcal{T} := (\mathcal{V}, \mathcal{E}_T)$, such that $\mathcal{E}_F \subseteq \mathcal{E}_T \subseteq \mathcal{E}$.

In other words, some edges may be removed from a spanning tree to obtain a spanning forest. This idea is illustrated in fig. 2. The solid lines show edges in a spanning forest and the addition of dashed edges creates a spanning tree. Hence, the radiality of $\mathcal{G}' := (\mathcal{V}, \mathcal{E}')$ holds true if there exists a fictitious spanning tree subgraph $\mathcal{T} := (\mathcal{V}, \mathcal{E}_T)$ of $\mathcal{G}$ such that $\mathcal{E}' \subseteq \mathcal{E}_T$. Let us first establish a condition to select a spanning tree, and then extract the required spanning forest from it. The base topology of $\mathcal{G}$ may be captured by a branch-bus incidence matrix $\tilde{\mathbf{A}}$ of dimension $|\mathcal{E}| \times (|\mathcal{V}|)$, with the following entries:

$$\tilde{\mathbf{A}}_{e_{ij},k} := \begin{cases} 1, & k = i \\ -1, & k = j \\ 0, & \text{otherwise} \end{cases} \tag{11}$$

The first column $\mathbf{a}_1$ of $\tilde{\mathbf{A}}$ may be separated as $\tilde{\mathbf{A}} = [\mathbf{a}_1\ \mathbf{A}]$. This yields the *reduced* branch-bus incidence matrix $\mathbf{A}$ of $\mathcal{G}$. An efficient model for imposing graph connectivity put forth in [33] posits that a graph with vertex set $\mathcal{V}$ and reduced branch-bus incidence matrix $\mathbf{A}$, is connected if and only if there exists a vector $\mathbf{f} \in \mathbb{R}^{|\mathcal{E}|}$, such that $\mathbf{A}^T\mathbf{f} = \mathbf{1}$. For proof, see [33].

For a physical interpretation, consider every vertex in $\mathcal{V} \setminus \{1\}$ injects unit virtual commodity into the network represented by the graph. Then, $\mathbf{f}$ denotes the flow of commodities on the edges. If this flow setup is feasible, then there must be a withdrawal of $|\mathcal{V}| - 1$ units at vertex 1, and every vertex in $\mathcal{V} \setminus \{1\}$ must have a path to reach vertex 1. Vertex 1 may be arbitrarily chosen.

Stating a well-known result from graph theory, a tree with n vertices has exactly $n - 1$ edges. Hence, the radiality constraints are stated as:

$$\mathbf{A}^T\mathbf{f} = \mathbf{1} \tag{12a}$$

$$-(|\mathcal{V}| - 1)\boldsymbol{\theta} \leq \mathbf{f} \leq (|\mathcal{V}| - 1)\boldsymbol{\theta}, \tag{12b}$$

$$\boldsymbol{\theta} \in \{0, 1\}^{|\mathcal{E}|} \tag{12c}$$

$$\mathbf{1}^T\boldsymbol{\theta} = |\mathcal{V}| - 1 \tag{12d}$$

$$\mathbf{b}^{\mathbf{e}} \leq \boldsymbol{\theta} \tag{12e}$$

Constraints (12a)-(12d) ensure that auxiliary binary indicator variables $\boldsymbol{\theta}$ on the edge-set of the base graph describe a spanning tree. Then, (12e) states that the edges selected via the binary variables $\mathbf{b}^{\mathbf{e}}$ are a subset of this spanning tree; and hence form a spanning forest structure as per Proposition 1. As the radiality constraints are thus posed, the number of components in $\mathcal{G}'$ need not be pre-assigned.

D. CONNECTION TO GRID-FORMING GENERATORS

As stated in Section I, the IEEE 1547 standard mandates that every viable microgrid should have a grid-forming generator that provides voltage and frequency support when isolated from the main grid. In practice, such a unit could be a CHP, a DG, or an inverter-interfaced PV generator with storage.

In the ODNP formulation described in this work, it is guaranteed that every energized bus in the network is connected to a grid-forming generator, or alternatively every microgrid has at least one grid-forming unit. Let $\mathcal{V}_s$ be the set of buses with grid-forming capabilities. Then, the connectivity constraints may be states as follows:

$$\sum_{e_{jk} \in \mathcal{E}} f'_{jk} - \sum_{e_{ij} \in \mathcal{E}} f'_{ij} = b^n_j, \quad \forall j \in \mathcal{V} \setminus \mathcal{V}_s \tag{13a}$$

$$-(|\mathcal{V}| - |\mathcal{V}_s|)\mathbf{b}^{\mathbf{e}} \leq \mathbf{f}' \leq (|\mathcal{V}| - |\mathcal{V}_s|)\mathbf{b}^{\mathbf{e}} \tag{13b}$$

Constraint (13a) states that every energized non grid-forming node in $\mathcal{G}$ injects unit virtual commodity into the network. Constraint (13b) bounds flows on energized lines and fixes flows on de-energized ones at 0. Here, $\mathbf{f}' \in \mathbb{R}^{|\mathcal{E}|}$ is a vector representing virtual line flows. It must be emphasized that $\mathbf{f}'$ is different from $\mathbf{f}$ in (12a). Both these vectors are used to impose connectivity conditions, and have no physical significance related to the power flow quantities. Again, this

setup is feasible only when all units injected by energized non grid-forming nodes can be withdrawn at grid-forming nodes.

Some grid-forming nodes may not be energized in the optimal topology. This is implicitly considered through the topological constraint in (1), that ensures all edges connected to a de-energized node are de-energized as well. Therefore, no path exists from an energized non grid-forming to a de-energized grid-forming node. A potential microgrid candidate may host multiple generators with grid-forming capabilities. In such cases, only one generator shall serve as the master unit, and suitable power sharing strategies may be required; see [34] and references therein.

E. DETERMINISTIC ODNP

The deterministic ODNP problem (d-ODNP) is solved for one realization of the power generation capacity ($\boldsymbol{\xi}^{g_p}, \boldsymbol{\xi}^{g_q}$), and demands ($\boldsymbol{\xi}^{d_p}, \boldsymbol{\xi}^{d_q}$). The central idea is to sustain maximum load through microgrids if supply from the main grid is lost, thereby minimizing service interruption. Therefore, the objective for d-ODNP becomes maximizing load served. The entire deterministic optimization setup may be mathematically expressed as follows.

$$\begin{aligned} &\min -\mathbf{1}^T \mathbf{p^d} \\ &\text{s. to } (1)-(9), (12a)-(12e), (13a)-(13b) \end{aligned} \quad \text{(ODNP-1)}$$

The relative priority of loads has not been considered in (ODNP-1). However, this cost may be modified by assigning weights to loads in proportion to their criticality.

F. PROBABILISTIC ODNP

The problem (ODNP-1) applies to one realization of the generation-demand scenario ($\boldsymbol{\xi}^{g_p}, \boldsymbol{\xi}^{g_q}, \boldsymbol{\xi}^{d_p}, \boldsymbol{\xi}^{d_q}$). However, a more realistic goal would be to identify microgrids that are optimal in some sense for a large set of realizations of the generation-demand scenarios. In the latter setup, the decision variables $\boldsymbol{\psi}_1 := \{\mathbf{b^n}, \mathbf{b^e}, \mathbf{f}, \mathbf{f'}, \boldsymbol{\theta}\}$ shall remain fixed for all realizations of the uncertainties. The realization dependent variables would be $\boldsymbol{\psi}_2 := \{\mathbf{p^d}, \mathbf{q^d}, \mathbf{p^g}, \mathbf{q^g}, \mathbf{v}, \mathbf{P}, \mathbf{Q}\}$. Collecting all the uncertainties in $\boldsymbol{\xi} := \{\boldsymbol{\xi}^{g_p}, \boldsymbol{\xi}^{g_q}, \boldsymbol{\xi}^{d_p}, \boldsymbol{\xi}^{d_q}\}$, the probabilistic ODNP may seek to solve-

$$\begin{aligned} &\min_{\boldsymbol{\psi_1}} \quad -\mathbb{E}_{\boldsymbol{\xi}}[\mathbf{1}^T \mathbf{p^d}] \\ &\text{s. to } \Pr\left(\exists\, \boldsymbol{\psi_2} | \mathbb{1}((1)-(9), (12a)-(13b)) = 1\right) \\ &\qquad \geq 1-\epsilon \end{aligned} \quad \text{(ODNP-2)}$$

The probabilistic constraint in (ODNP-2) is very difficult to enforce in practice. However, we will next discuss some reformulations that simplify the setup without loss of generality. First, note that if the power demands at all nodes are zero, then for a feasible $\boldsymbol{\psi}_1$ satisfying (1) and (12a)-(13b), there always exists a $\boldsymbol{\psi}_2$ that satisfies all other constraints. Therefore, the probabilistic constraint may be equivalently posed by enforcing all constraints other than (6a)-(6b) as hard constraints, and putting the probabilistic requirement on (6a)-(6b). Setting aside (6b) for expository convenience, notice that the equality constraints in (6a) may be decomposed into the following inequality constraints.

$$p_i^d - b_i^n \xi_i^{d_p} \leq 0, \quad \forall i \tag{14a}$$

$$-p_i^d + b_i^n \xi_i^{d_p} \leq 0, \quad \forall i \tag{14b}$$

Now, (14a) can be posed as a hard constraint, leaving (14b) as the main chance constraint. To reiterate, the ODNP task seeks to identify potential microgrids within an existing distribution network, such that load served is maximized, and the microgrids are self-adequate with probability at least $(1-\varepsilon)$. Islanded microgrids are called self-adequate when their internal load can be met by their internal generation. Mathematically,

$$Pr(-p_i^d + b_i^n \xi_i^{d_p} \leq 0, \forall i) \geq 1-\varepsilon \tag{15}$$

The self-adequacy condition of microgrids can hence be posed at the node level since constraints (12a)-(12e) ensure that the network topology is a spanning forest, and loads in a microgrid can be supplied only by generators within the same microgrid. If needed, one may relax the the reliability requirement by modifying (15) slightly. For instance, the condition that a microgrid should be able to serve 90% of its internal load could be written as $Pr(-p_i^d + 0.9 \times b_i^n \xi_i^{d_p} \leq 0, \forall i) \geq 1-\varepsilon$.

G. SAMPLE AVERAGE APPROXIMATION

Recall from Section III-B that a chance constraint needs to be satisfied with a probability specified by a risk parameter ε. The chance-constraint (C_2) may also be rewritten as $q(\boldsymbol{x}) \leq \varepsilon$, where $q(\boldsymbol{x}) = Pr(\boldsymbol{g}(\boldsymbol{x}, \boldsymbol{\xi}) > \mathbf{0})$. Let $\boldsymbol{\xi^1}, \boldsymbol{\xi^2}, \ldots, \boldsymbol{\xi^N}$ be N independent and identically distributed (iid) samples of the uncertainty vector $\boldsymbol{\xi}$; then $\hat{q_N}(\boldsymbol{x})$, an estimator of $q(\boldsymbol{x})$ is equal to the proportion of realizations in the sample where $\boldsymbol{g}(\boldsymbol{x}, \boldsymbol{\xi^i}) > \mathbf{0}, i = 1, .., N$. This is a sample average approximation of the chance-constrained problem (P_1) for the samples $\boldsymbol{\xi^1}, \boldsymbol{\xi^2}, \ldots, \boldsymbol{\xi^N}$:

$$\min_{\boldsymbol{x} \in \mathcal{X}} f(\boldsymbol{x}) \quad \text{s.to. } \hat{q_N}(\boldsymbol{x}) \leq \gamma \tag{P_2}$$

Here, $\gamma \in (0, 1)$ and is the risk level for the SAA problem. Assuming that the SAA can be solved, a) if $\gamma < \varepsilon$, and N is sufficiently large, SAA is a restriction on the true problem and a feasible solution of SAA is likely to be feasible for the true problem as well, b) if $\gamma > \varepsilon$, SAA is a relaxation of the true problem and the optimal value of SAA is likely to be a lower bound to the optimum for true problem. It can be shown that for $\gamma = \varepsilon$, the SAA optimum approaches its true counterpart with probability one as N approaches infinity [21].

The chance-constrained SAA problem P_2 can be solved using MILP for N iid samples of $\boldsymbol{\xi}$ as shown below [21].

$$\min_{\boldsymbol{x}\in\mathcal{X}} f(\boldsymbol{x}) \tag{P_3}$$
$$\text{s. to } \boldsymbol{h}(\boldsymbol{x}) \leq \mathbf{0} \tag{16a}$$
$$\boldsymbol{g}(\boldsymbol{x}, \boldsymbol{\xi}^{\alpha}) \leq M(1 - z_{\alpha}), \quad \alpha = 1, 2, \ldots, N \tag{16b}$$
$$\mathbf{1}^T\mathbf{z} \geq (1-\gamma)N \tag{16c}$$
$$\mathbf{z} \in \{0,1\}^N, \quad \alpha = 1, 2, \ldots, N \tag{16d}$$

Here, α is used to index samples of $\boldsymbol{\xi}$, z_α is a binary variable and M is a large number such that $M > \max_{\boldsymbol{x}\in\mathcal{X}} \boldsymbol{g}(\boldsymbol{x}, \boldsymbol{\xi}^{\alpha})$ for all $\alpha = 1, 2, \ldots, N$. Vector $\mathbf{z}$ stacks all z_α values. In constraint (16b), if $z_\alpha = 1$, then the chance constraint is not violated. If $z_\alpha = 0$, then no bound is imposed. The cardinality constraint in (16c) bounds the proportion of constraint violations.

For ODNP the hard constraints are given by $\{(1)-(4b), (6b)-(9), (12a)-(13b), (14a)\ \forall\alpha\}$. Probability of violating the chance-constraint $\{(14b)\ \forall\alpha\}$ is to be bounded. Equation (16b) becomes:

$$-\mathbf{p^d}_{\alpha} + diag(\mathbf{b^n}) \times \boldsymbol{\xi}^{\mathbf{d_p},\alpha} \leq M(1 - z_{\alpha}) \times \mathbf{1}, \quad \forall\alpha \tag{17}$$

Putting everything together, the problem becomes:

$$\min \ -\frac{1}{N}\sum_{\alpha=1}^{N} \mathbf{1}^T\mathbf{p^d}_{\alpha} \tag{ODNP-3}$$
$$\text{s. to } \mathbf{p^d}_{\alpha} \leq z_{\alpha} \times \boldsymbol{\xi}^{\boldsymbol{d_p}}, \quad \forall\alpha$$
$$(1) - (4b), (12a) - (13b), (14a), (16c) - (17) \tag{18}$$

The objective function in (ODNP-3) is the sample-based estimator of the objective in (ODNP-2) designed to maximize average load served across considered scenarios. Constraint (18) fixes bus consumptions at zero when constraint (14b) is not satisfied. This motivates the optimal solution for the ODNP to be one that also increases $\mathbf{1}^T\mathbf{z}$, lower bounded by $(1-\gamma)N$.

The optimal topology obtained by solving (ODNP-3) is determined by vectors $\mathbf{b^{n*}}$ and $\mathbf{b^{e*}}$. In practice, microgrids can be isolated by opening the boundary lines between energized nodes and deenergized nodes.

V. SOLUTION VALIDATION

Consider a candidate solution $\bar{\boldsymbol{x}}$ found by the SAA approach of (ODNP-3). To adjudge its quality, two aspects need to be analyzed: *a)* Can it be said with some desired confidence that $\bar{\boldsymbol{x}}$ a feasible solution for the true problem (ODNP-2)? *b)* If yes, then how far is $f(\bar{\boldsymbol{x}})$ from the optimal value $f(\boldsymbol{x}^*)$? A method for checking an upper bound of $Pr\{\boldsymbol{g}(\bar{\boldsymbol{x}}, \boldsymbol{\xi}) > \mathbf{0}\}$ and lower bound on $f(\boldsymbol{x}^*)$ is shown in [21] and references therein.

A. UPPER BOUND ON VIOLATION PROBABILITY

Consider N' iid realizations of $\boldsymbol{\xi}$, such that $N' \gg N$, where N is the number of $\boldsymbol{\xi}$ samples used for solving the SAA problem. Here, N' may be large as the samples will not be used in solving an optimization problem, avoiding computational issues. Let $\hat{q}_{N'}(\bar{\boldsymbol{x}})$ be an estimator of $q(\bar{\boldsymbol{x}})$; equal to the proportion of times the event $\mathbb{1}(\boldsymbol{g}(\bar{\boldsymbol{x}}, \boldsymbol{\xi}^{\boldsymbol{j}}) > \mathbf{0}) = 1$ is observed in N' trials. Estimator $\hat{q}_{N'}(\bar{\boldsymbol{x}})$ of $q(\bar{\boldsymbol{x}})$ is unbiased, implying $\mathbb{E}(\hat{q}_{N'}(\bar{\boldsymbol{x}})) = q(\bar{\boldsymbol{x}})$. Also, for a large N', its distribution may be approximated by a normal distribution with mean $q(\bar{\boldsymbol{x}})$ and variance $q(\bar{\boldsymbol{x}})(1 - q(\bar{\boldsymbol{x}}))/N'$ [21]. This yields an approximate $(1-\beta)$-confidence upper bound on $q(\bar{\boldsymbol{x}})$:

$$U_{\beta,N'}(\bar{\boldsymbol{x}}) := \hat{q}_{N'}(\bar{\boldsymbol{x}}) + z_{\beta}\sqrt{\hat{q}_{N'}(\bar{\boldsymbol{x}})(1 - \hat{q}_{N'}(\bar{\boldsymbol{x}}))/N'} \tag{19}$$

Here, $z_\beta = \Phi^{-1}(1-\beta)$, where Φ is the cumulative distribution function for the standard normal distribution, $\beta \in (0, 1)$. We compare $U_{\beta,N'}(\bar{\boldsymbol{x}})$ to ε to check if $\bar{\boldsymbol{x}}$ is a feasible solution. If $U_{\beta,N'}(\bar{\boldsymbol{x}}) \leq \varepsilon$, then $\bar{\boldsymbol{x}}$ describes a topology where microgrids are very likely to be self-sufficient. A summary of the steps to be followed to derive this upper bound on chance constraint violation probability is provided in algorithm 1. Note that the scenarios used to solve and validate the SAA problem are generated using independent processes.

Algorithm 1 Derivation of Upper Bound on Chance Constraint Violation Probability

1. Generate N' iid realizations of $\boldsymbol{\xi}$, where $N' \gg N$.
2. For the N' scenarios, count the number of times (N'_v) the event $\mathbb{1}(\boldsymbol{g}(\bar{\boldsymbol{x}}, \boldsymbol{\xi}^{\boldsymbol{j}}) > \mathbf{0}) = 1$ is observed.
3. Calculate $\hat{q}_{N'}(\bar{\boldsymbol{x}}) = N'_v/N'$.
4. Substitute $\hat{q}_{N'}(\bar{\boldsymbol{x}})$ in equation (19) and calculate $U_{\beta,N'}(\bar{\boldsymbol{x}})$.

B. LOWER BOUND ON OPTIMAL VALUE

A procedure for deriving a lower bound for $f(\boldsymbol{x}^*)$ is shown in [21]. Let the SAA problem (ODNP-3) be solved for N'' iid samples of $\boldsymbol{\xi}$ with risk level $\gamma \geq 0$; and denote this problem by $P_{\gamma}^{N''}$. Let the true problem (ODNP-2) with risk ε be denoted as P_{ε}. Now, the probability that at most $\lfloor \gamma N'' \rfloor$ constraint violations are observed in N'' trials while solving $P_{\gamma}^{N''}$, when the true violation probability is ε, becomes:

$$\Theta_{N''} := B(\lfloor \gamma N'' \rfloor; \varepsilon, N'')$$

where,

$$B(k; q, N) := \sum_{r=0}^{k-1} \binom{N}{r} q^r (1-q)^{N-r}$$

is the cumulative density function of the binomial distribution. Say, solving $P_{\gamma}^{N''}$ yields an objective value $f(\bar{\boldsymbol{x}})$. Assuming P_ε has an optimal solution $f(\boldsymbol{x}^*)$, $Pr\{f(\bar{\boldsymbol{x}}) \leq f(\boldsymbol{x}^*)\} \geq \Theta''_N$. This result yields a method for obtaining lower bounds with a specified confidence level $(1-\beta)$.

Consider two positive integers M and N'', such that $M > N''$. Generate M independent sets of N'' iid samples of $\boldsymbol{\xi}$, and solve the SAA problem for each of the M sets to obtain values $f(\bar{\boldsymbol{x}})_j, j = 1, 2, \ldots, M$. These can be viewed as iid samples of the random variable $f(\bar{\boldsymbol{x}})$. Let L be the largest integer such that

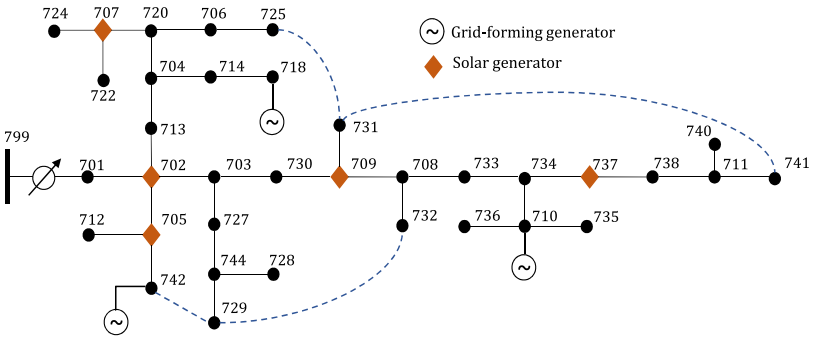

FIGURE 3. Modified IEEE 37-bus benchmark feeder showing the location of DER units and normally open switches.

Algorithm 2 Derivation of Lower Bound on Optimal Value

1. Choose two positive integers M and N'' such that $M > N''$. A guide for selection is provided in [35].
2. Generate M independent sets of N'' iid samples of $\boldsymbol{\xi}$. For each of the M sets, solve (ODNP-3) to obtain values $f(\bar{\boldsymbol{x}})_j, j = 1, 2, \ldots, M$.
3. Find the largest integer L such that $B(L-1; \Theta''_N, M) \leq \beta$.
4. Arrange the optimal values in a non-decreasing order $f(\bar{\boldsymbol{x}})_1 \leq f(\bar{\boldsymbol{x}})_2 \leq \cdots \leq f(\bar{\boldsymbol{x}})_M$. The lower bound for $f(\boldsymbol{x}^*)$ with confidence level $(1-\beta)$ is $f(\bar{\boldsymbol{x}})_L$.

$B(L-1; \Theta''_N, M) \leq \beta$. If the optimal values are arranged in a non-decreasing order $f(\bar{\boldsymbol{x}})_1 \leq f(\bar{\boldsymbol{x}})_2 \leq \ldots f(\bar{\boldsymbol{x}})_M$, it can be shown that with probability at least $(1-\beta)$, $f(\bar{\boldsymbol{x}})_L$ is lower than the true optimal value $f(\boldsymbol{x}^*)$.

Note that $f(\bar{\boldsymbol{x}})_L > f(\boldsymbol{x}^*)$ if and only if more than L of the observed $f(\bar{\boldsymbol{x}})_j$ values are greater than $f(\boldsymbol{x}^*)$. Considering event $f(\bar{\boldsymbol{x}})_j \leq f(\boldsymbol{x}^*)$ as a success, $f(\bar{\boldsymbol{x}})_L > f(\boldsymbol{x}^*)$ if and only if there are fewer than L successes in M trials, with success probability $\Theta_{N''}$. Probability of fewer than L successes in M trials is $B(L-1, \Theta_{N''}, M)$, and the bounding procedure described in this section restricts this probability value to β.

The steps for calculating the lower bound on $f(\bar{\boldsymbol{x}})$ with a confidence level of $(1-\beta)$ are summarized in algorithm 2. Further insights on validating the quality of solutions yielded by SAA problems are available in [21], [35] and references therein.

VI. NUMERICAL RESULTS

Performance of the proposed methodology is illustrated through computational experiments on a 3.6 GHz Intel Core i7-4790 CPU with 32 GB RAM. Optimization tasks are solved using YALMIP and Gurobi [36], [37].

A. EXPERIMENT SET-UP

The ODNP problem is solved for a modified version of the IEEE 37-bus benchmark feeder (fig. 3), converted to its single-phase equivalent by: a) assigning average three-phase load as bus spot-loads, and b) assigning average three-phase impedances as line impedances. Four normally open switches are added (shown with dotted edges in fig. 3). Grid-forming generators are placed at nodes 742, 718 and 710. PV generators of equal rated capacity (without grid-forming abilities) are added at nodes 702, 705, 707, 709 and 737. There are 22 buses with non-zero load. Total rated capacity of grid-forming and PV generators are 13% and 29% of the rated system load respectively. Practical feeders of the scale of our benchmark may not host such extensive distributed resources. However, such a model has been intentionally chosen to capture diverse flexibilities and computational concerns that may show up in real but larger networks. A feeder with fewer generators and tie-lines would have fewer load-generation scenarios and would be faster to solve for.

Load-generation scenarios were constructed as described next. Data corresponding to hourly solar generation in California from NREL's solar power dataset were used to synthesize five annual generation profiles [38]. The first 50 generators in the dataset were used; every 10 generators were aggregated to obtain one profile. The normalized profiles were then scaled to match the rated capacity of the generators. It is further assumed that the PV generators are set to work at unity power factor, implying that they do not participate in reactive power support. This is without loss of generality since PV generators with reactive power support may be indicated with non-zero entries in the $\boldsymbol{\xi}^{g_q}$ vector. In a similar manner, hourly load profiles were constructed for residential and commercial buildings in California with data available from OpenEI [39]. The normalized profiles were scaled such that the 75th percentile of load data coincided with the nominal spot load of the corresponding bus. Thus, a total of 8760 scenarios were constructed for a year; denoted as set $\mathcal{S}$.

B. CHANCE-CONSTRAINED ODNP

As stated previously, the original chance-constrained problem and its SAA counterpart become equivalent in limit as the number of scenarios considered N increases. However, a higher N value also increases computation time. This increasing trend is illustrated in fig. 6, the markers show median time for 10 runs conducted over the same

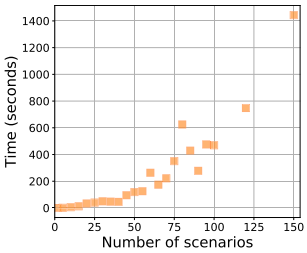

FIGURE 4. Median computation time increases with number of scenarios .

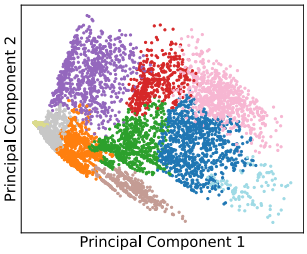

FIGURE 5. 2-D visualization of scenario clusters .

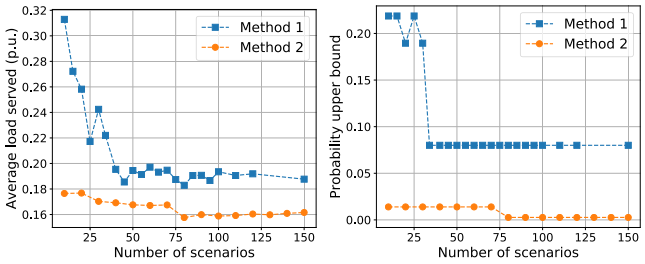

(a) Average load served (b) Constraint violation probability

FIGURE 6. Variation in performance when number of scenarios is varied from 10 to 150. Proposed cc-ODNP is compared to a clustering based method.

scenario sets. For computational tractability, let the SAA problem be solved on a smaller sample set $\mathcal{S}' \subseteq \mathcal{S}$; if $\mathcal{S}'$ is sufficiently representative of $\mathcal{S}$, then the candidate solution obtained will be close to the true solution for the original CCO problem.

Performance of the SAA approach is compared to a clustering based methodology, wherein set $\mathcal{S}$ is divided into clusters and the ODNP task is designed to yield a solution that holds for some representative samples drawn from these clusters. Let us call these two *Method 1* and *Method 2* respectively.

• *Method 1:* Scenarios are sampled from $\mathcal{S}$ at random with uniform probability and used to solve (ODNP-3).

• *Method 2:* Using principal component analysis followed by agglomerative hierarchical clustering, set $\mathcal{S}$ is divided into 10 clusters [40]. The scenario clusters are visualized in fig. 5. Once the clusters are determined, equal number of samples are randomly drawn from each cluster. Evidently, samples can only be drawn in multiples of 10. The ODNP is solved such that the optimal topology is feasible for all selected samples, i.e. $\gamma = 0$.

The performance of the two solution methods is compared in fig. 7. For SAA, the value of γ used is 0.1. A 95% confidence lower bound on the objective value is found using

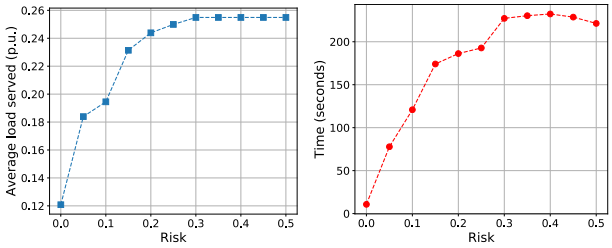

(a) Average load served (b) Median time taken for 10 runs

FIGURE 7. Variation in cc-ODNP performance with γ considering 50 scenarios.

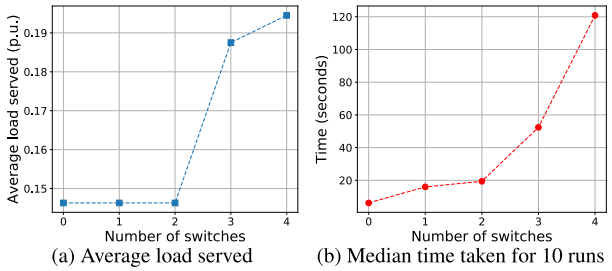

(a) Average load served (b) Median time taken for 10 runs

FIGURE 8. Variation in performance with number of normally open switches. Number of scenarios considered is 50, $\gamma = 0.1$.

TABLE 1. Comparison of SAA and Clustering Based Approaches.

	Method 1	Method 2
$\lvert\mathbf{f}(\bar{\mathbf{x}}) - \mathbf{f}(\mathbf{x}^*)\rvert$	0.00814	0.34416
$\mathbf{U}_{0.05,1000}(\bar{\mathbf{x}})$	0.08	0.0025

the methodology described in Section V. With 50 runs of independently generated sets of 20 scenarios each, and $\gamma = 0.7$, this lower bound is determined to be -0.18536. The parameters M, N'' and γ here were chosen following the recommendations outlined in [35]. The 95% confidence upper bound on feasibility of the candidate solution $U_{0.05,1000}(\bar{\mathbf{x}})$ is estimated using a set of 1000 scenarios. Median computation time for the feasibility checking process was 1.438 seconds.

Evidently, as more scenarios are considered, both average load served and $U_{0.05,1000}(\bar{\mathbf{x}})$ decrease. The trends are not strict as additional scenarios can introduce favorable cases with lower cost. Observe that Method 2 yields a more robust solution (low constraint violation probability) in lieu of a higher objective cost. Method 1 achieves an objective value close to the theoretical lower bound while bounding supply-deficiency probability to an acceptable level. Table 1 summarizes observations when both methods are run over 100 scenarios.

C. CHOICE OF RISK PARAMETER

The optimal topology is highly dependent on the specified risk parameter. Of course, if a utility has a high risk budget, they may plan to cover a larger amount of loads with microgrids. The risk appetite may be dictated by a number of factors, such as the installed storage capacity and criticality of loads. If the loads to be served are critical (hospitals, police stations etc), then the risk budget goes down. The intuition of higher load served with higher risk tolerance is

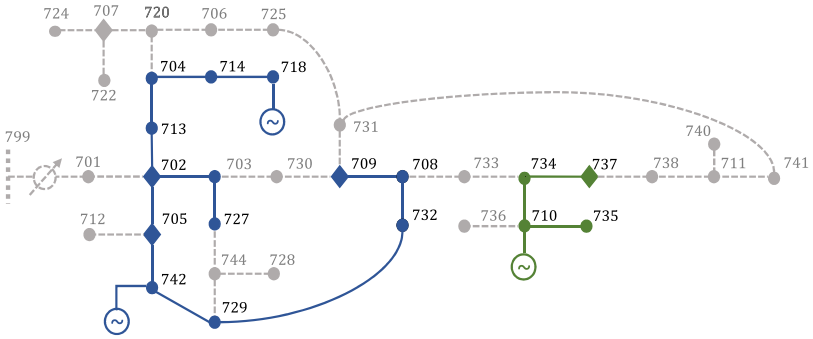

FIGURE 9. Optimal microgrid topology considering all switches, 100 scenarios and $\gamma = 0.1$. Average load served is 0.1935 p.u.. $U_{0.05,1000}(\bar{\mathbf{x}}) = 0.08005$.

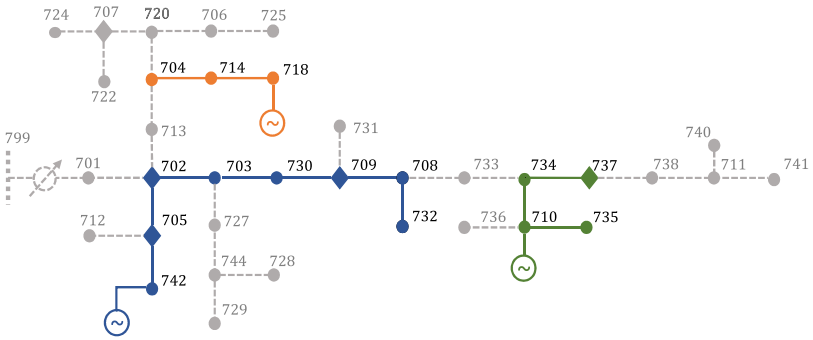

FIGURE 10. Optimal microgrid topology for the base radial network, 100 scenarios and $\gamma = 0.1$. Average load served is 0.1483 p.u.. $U_{0.05,1000}(\bar{\mathbf{x}}) = 0.06465$.

experimentally verified and shown in fig.7. It can also be seen that computation time increases with γ; possibly because for higher values of γ, the feasibility space that the solver has to search for an optimal solution to ODNP grows in size.

D. NUMBER OF NORMALLY OPEN SWITCHES

Any topology determination problem is combinatorial in nature, and hence the search space and solution time increases with the number of graph edges. In the ODNP task, network flexibility may be better utilized to serve more load by leveraging normally open switches. However, addition of extra edges introduces additional binary decision variables, thereby increasing solution time. In fig. 8, it is shown that as more switches are added to the base radial 37-bus network, ODNP yields higher average load served (i.e. lower objective values), but the computation time grows. These data points were determined by solving the ODNP problem over 50 scenarios sampled with method 1 and using $\gamma = 0.1$. For each of these cases, multiple combinations of normally open switches are possible. However, switches were added one at a time in a random sequence to the base network for illustration.

E. MICROGRID TOPOLOGY

Optimal microgrids determined for the base radial network with and without normally open switches are shown in fig. 9 and 10 respectively. Microgrid components are indicated in color while external elements are in grey. When all switches are considered, higher load can be served. When only the base radial network is considered, load served by microgrids is lower, and so is the supply-deficiency violation probability.

The determined microgrids do not violate the self-adequacy and power systems constraints for more than γ fraction of cases, are radial and contain at least one grid-forming generator. Notice that despite hosting a solar generator, bus 707 is not included in any of the microgrids. This may be because there are no possible ways to connect bus 707 to a grid-forming generator without violating one of the prescribed constraints.

F. COMPUTATIONAL PERFORMANCE

As illustrated in the simulated examples, the time required to solve the stochastic ODNP problem depends on several factors such as network size, number of scenarios considered, number of switches and the choice of risk parameter. Evidently, the inherent combinatorial and stochastic nature of the underlying network splitting problem poses computational challenges. Fortunately, since ODNP is a planning problem, the scalability concern is less severe compared to similar applications pertaining to real-time operation. Nevertheless, to enhance scalability, the linearized distribution flow model [31] is used in this work instead of the full AC power flow model, thus yielding a MILP formulation. Recent advancements in commercial solvers like CPLEX and Gurobi have significantly improved both the speed and scale at which MILPs can be solved. This makes MILP formulations attractive even for operation problems like topology reconfiguration, and well-suited for planning-stage ODNP.

Thus, the computational burden for solving ODNP is not prohibitive and can be used to identify potential microgrids in large distribution feeders with high DER penetration.

VII. CONCLUSION

The power grid is critical for maintaining essential sectors like healthcare, transportation and emergency services. This has motivated research towards enhancing grid resilience, and formulating measures to hedge against extreme events. Efficiently planned microgrids can help minimize load interruptions and aid restoration during and after large-scale outages. To this end, this work proposes a chance-constrained optimal network partitioning problem and presents a computationally tractable solution methodology. Specifically, the ODNP problem seeks to enhance resilience by improving grid performance in the post-disaster degraded state.

First, a deterministic version of the ODNP problem is formulated considering practical constraints such as maintaining network radiality and the availability of grid-forming generators. The optimal network topology is determined without pre-fixing the number of partitions, or pre-assigning DERs to microgrids. Moreover, the requirement of grid-forming generators in viable islands had not been addressed in prior microgrid planning literature. Next, the deterministic problem is extended to a probabilistic setup to account for the stochasticity in energy demand and renewable energy generation. The probabilistic optimization problem is solved using sample average approximation. Further, the article discusses how to assess the quality of the obtained SAA solution using rigorous statistical tools.

Case-studies on a modified version of the IEEE 37-bus feeder show that good quality candidate solutions can be found with modest computation cost; network flexibility is well-utilized; and partitioning changes with risk budget. Future work will focus on extending the present planning-stage formulations to multi-phase topologies and near real-time applications.

REFERENCES

[1] K. P. Schneider, F. K. Tuffner, M. A. Elizondo, C.-C. Liu, Y. Xu, and D. Ton, "Evaluating the feasibility to use microgrids as a resiliency resource," *IEEE Trans. Smart Grid*, vol. 8, no. 2, pp. 687–696, Mar. 2017.

[2] *IEEE Guide for Design, Operation, and Integration of Distributed Resource Island Systems with Electric Power Systems*, IEEE Standard 1547.4-2011, 2011.

[3] U. S. Department of Energy, "How distributed energy resources improve resilience in public buildings: Three case studies," U.S. Dept. Energy, Washington, DC, USA, Tech. Rep., Sep. 2019. [Online]. Available: https://www.energy.gov/eere/slsc/downloads/how-distributed-energy-resources-can-improve-resilience-public-buildings-three

[4] *Modeling the Impact of Flexible CHP on California's Future Electric Grid*, U.S. Dept. Energy, Washington, DC, USA, Jan. 2018.

[5] *Enhancing Grid Resilience With Integrated Storage From Electric Vehicles*, U.S. Dept. Energy, Washington, DC, USA, Jun. 2018.

[6] B. Zeng, J. Feng, N. Liu, and Y. Liu, "Co-optimized parking lot placement and incentive design for promoting PEV integration considering decision-dependent uncertainties," *IEEE Trans. Ind. Informat.*, vol. 17, no. 3, pp. 1863–1872, Mar. 2021.

[7] H. Gao, Y. Chen, S. Mei, S. Huang, and Y. Xu, "Resilience-oriented pre-hurricane resource allocation in distribution systems considering electric buses," *Proc. IEEE*, vol. 105, no. 7, pp. 1214–1233, Jul. 2017.

[8] F. Noor, R. Arumugam, and M. Vaziri, "Unintentional islanding and comparison of prevention techniques," in *Proc. 37th Annu. North Amer. Power Symp.*, Ames, IA, USA, 2005, pp. 90–96.

[9] S. Lei, C. Chen, Y. Song, and Y. Hou, "Radiality constraints for resilient reconfiguration of distribution systems: Formulation and application to microgrid formation," *IEEE Trans. Smart Grid*, vol. 11, no. 5, pp. 3944–3956, Sep. 2020.

[10] T. Ding, Y. Lin, G. Li, and Z. Bie, "A new model for resilient distribution systems by microgrids formation," *IEEE Trans. Power Syst.*, vol. 32, no. 5, pp. 4145–4147, Sep. 2017.

[11] Z. Wang and J. Wang, "Self-healing resilient distribution systems based on sectionalization into microgrids," *IEEE Trans. Power Syst.*, vol. 30, no. 6, pp. 3139–3149, Nov. 2015.

[12] R. Jovanovic, A. Bousselham, and S. Voß, "Partitioning of supply/demand graphs with capacity limitations: An ant colony approach," *J. Combinat. Optim.*, vol. 35, no. 1, pp. 224–249, Jan. 2018.

[13] R. A. Osama, A. F. Zobaa, and A. Y. Abdelaziz, "A planning framework for optimal partitioning of distribution networks into microgrids," *IEEE Syst. J.*, vol. 14, no. 1, pp. 916–926, Mar. 2020.

[14] S. A. Arefifar, Y. A.-R.-I. Mohamed, and T. H. M. El-Fouly, "Supply-adequacy-based optimal construction of microgrids in smart distribution systems," *IEEE Trans. Smart Grid*, vol. 3, no. 3, pp. 1491–1502, Sep. 2012.

[15] M. E. Nassar and M. M. A. Salama, "Adaptive self-adequate microgrids using dynamic boundaries," *IEEE Trans. Smart Grid*, vol. 7, no. 1, pp. 105–113, Jan. 2016.

[16] C. Chen, J. Wang, F. Qiu, and D. Zhao, "Resilient distribution system by microgrids formation after natural disasters," *IEEE Trans. Smart Grid*, vol. 7, no. 2, pp. 958–966, Mar. 2016.

[17] M. Barani, J. Aghaei, M. A. Akbari, T. Niknam, H. Farahmand, and M. Korpas, "Optimal partitioning of smart distribution systems into supply-sufficient microgrids," *IEEE Trans. Smart Grid*, vol. 10, no. 3, pp. 2523–2533, May 2019.

[18] S. Biswas, E. Bernabeu, and D. Picarelli, "Proactive islanding of the power grid to mitigate high-impact low-frequency events," in *Proc. IEEE Power Energy Soc. Innov. Smart Grid Technol. Conf. (ISGT)*, Washington, DC, USA, Feb. 2020, pp. 1–5.

[19] M. K. Singh, V. Kekatos, and C.-C. Liu, "Optimal distribution system restoration with microgrids and distributed generators," in *Proc. IEEE Power Energy Soc. Gen. Meeting (PESGM)*, Atlanta, GA, USA, Aug. 2019, pp. 1–5.

[20] G. Patsakis, D. Rajan, I. Aravena, and S. Oren, "Strong mixed-integer formulations for power system islanding and restoration," *IEEE Trans. Power Syst.*, vol. 34, no. 6, pp. 4880–4888, Nov. 2019.

[21] S. Ahmed and A. Shapiro, "Solving chance-constrained stochastic programs via sampling and integer programming," in *State-of-the-Art Decision-Making Tools in the Information-Intensive Age*. Catonsville, MD, USA: Informs, 2008, pp. 261–269.

[22] M. Panteli, P. Mancarella, D. N. Trakas, E. Kyriakides, and N. D. Hatziargyriou, "Metrics and quantification of operational and infrastructure resilience in power systems," *IEEE Trans. Power Syst.*, vol. 32, no. 6, pp. 4732–4742, Nov. 2017.

[23] H. Gao, Y. Chen, Y. Xu, and C.-C. Liu, "Resilience-oriented critical load restoration using microgrids in distribution systems," *IEEE Trans. Smart Grid*, vol. 7, no. 6, pp. 2837–2848, Nov. 2016.

[24] S. Mohebbi, Q. Zhang, E. Christian Wells, T. Zhao, H. Nguyen, M. Li, N. Abdel-Mottaleb, S. Uddin, Q. Lu, M. J. Wakhungu, Z. Wu, Y. Zhang, A. Tuladhar, and X. Ou, "Cyber-physical-social interdependencies and organizational resilience: A review of water, transportation, and cyber infrastructure systems and processes," *Sustain. Cities Soc.*, vol. 62, Nov. 2020, Art. no. 102327.

[25] *IEEE Guide for Electric Power Distribution Reliability Indices*, IEEE Standard 1366-2012, (Revision IEEE Std 1366-2003), 2012, pp. 1–43.

[26] C. Godsil and G. Royle, *Algebraic Graph Theory*. New York, NY, USA: Springer, 2001.

[27] X. Geng and L. Xie, "Data-driven decision making in power systems with probabilistic guarantees: Theory and applications of chance-constrained optimization," *Annu. Rev. Control*, vol. 47, pp. 341–363, May 2019.

[28] *American National Standard for Electric Power Systems and Equipment—Voltage Ratings (60 Hertz)*, ANSI Standard C84.1-1995, 2016.

[29] R. A. Jabr, "Linear decision rules for control of reactive power by distributed photovoltaic generators," *IEEE Trans. Power Syst.*, vol. 33, no. 2, pp. 2165–2174, Mar. 2018.

[30] M. E. Baran and F. F. Wu, "Network reconfiguration in distribution systems for loss reduction and load balancing," *IEEE Trans. Power Del.*, vol. 4, no. 2, pp. 1401–1407, Apr. 1989.
[31] S. Bolognani and F. Dorfler, "Fast power system analysis via implicit linearization of the power flow manifold," in *Proc. 53rd Annu. Allerton Conf. Commun., Control, Comput. (Allerton)*, Allerton, IL, USA, Sep. 2015, pp. 402–409.
[32] G. P. McCormick, "Computability of global solutions to factorable nonconvex programs: Part I—Convex underestimating problems," *Math. Program.*, vol. 10, no. 1, pp. 147–175, Dec. 1976.
[33] M. K. Singh, V. Kekatos, S. Taheri, K. P. Schneider, and C.-C. Liu, "Enforcing radiality constraints for DER-aided power distribution grid reconfiguration," 2019, *arXiv:1910.03020*. [Online]. Available: https://arxiv.org/abs/1910.03020
[34] S.-J. Ahn, J.-W. Park, I.-Y. Chung, S.-I. Moon, S.-H. Kang, and S.-R. Nam, "Power-sharing method of multiple distributed generators considering control modes and configurations of a microgrid," *IEEE Trans. Power Del.*, vol. 25, no. 3, pp. 2007–2016, Jul. 2010.
[35] A. Nemirovski and A. Shapiro, "Convex approximations of chance constrained programs," *SIAM J. Optim.*, vol. 17, no. 4, pp. 969–996, Jan. 2007.
[36] J. Löfberg, "YALMIP: A toolbox for modeling and optimization in MATLAB," in *Proc. IEEE Int. Conf. Robot. Autom.*, Taipei, Taiwan, Sep. 2004, pp. 284–289.
[37] *Gurobi Optimizer Ref. Manual*, Gurobi Optim. LLC, Beaverton, OR, USA, 2020.
[38] NREL. *Solar Power Data for Integration Studies*. Accessed: Dec. 15, 2020. [Online]. Available: https://www.nrel.gov/grid/solar-power-data.html
[39] OpenEI. *Commercial and Residential Hourly Load Profiles for All TMY3 Locations in the United States*. Accessed: Dec. 15, 2020. [Online]. Available: https://openei.org/datasets/files/961/pub/
[40] P.-N. Tan, M. Steinbach, and V. Kumar, *Introduction to Data Mining*. Reading, MA, USA: Addison-Wesley, 2005.

SHUCHISMITA BISWAS (Graduate Student Member, IEEE) received the B.Tech. degree in electrical engineering from NIT Durgapur, India, in 2014, and the M.S. degree in electrical engineering from Virginia Tech, Blacksburg, VA, USA, in 2018, where she is currently pursuing the Ph.D. degree. She was an Application Engineer with the Medium Voltage Switchgear Division, Schneider Electric India, from 2014 to 2016. She has also been a Summer Intern with the Pacific Northwest National Laboratory, Richland, WA, USA, and PJM Interconnection, Audubon, PA, USA. Her research interest includes using optimization and data analysis tools for enhancing power systems resilience.

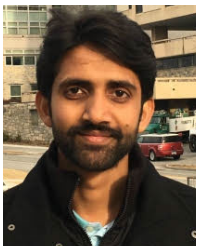

MANISH K. SINGH (Graduate Student Member, IEEE) received the B.Tech. degree in electrical engineering from IIT (BHU) Varanasi, Varanasi, India, in 2013, and the M.S. degree in electrical engineering from Virginia Tech, Blacksburg, VA, USA, in 2018, where he is currently pursuing the Ph.D. degree. From 2013 to 2016, he was an Engineer with the Smart Grid Department, POWERGRID, the central transmission utility of India. His research interests include the application of learning, optimization, control, and graph-theoretic techniques to develop algorithmic solutions for operation and analysis of water, natural gas, and electric power systems.

VIRGILIO A. CENTENO (Senior Member, IEEE) received the M.S. and Ph.D. degrees in electrical engineering from Virginia Polytechnic Institute and State University (Virginia Tech), Blacksburg, VA, USA, in 1988 and 1995, respectively. From 1991 to 1997, he was a Project Engineer in the development of phasor measurement units with Macrodyne, Inc., Clifton Park, NY, USA. In Fall of 1997, he joined the Faculty of Virginia Tech as a Visiting Professor, where he became an Associate Professor in 2007. His research interest includes wide-area measurement and its applications to power system protection and control.